Imaging through curved glass: Windshield optical impact on automotive cameras

Korbinian Weikl[a,b], Jeppe Revall Frisvad[c], Damien Schroeder[b], and Walter Stechele[a]

[a]Technical University of Munich, Arcisstrasse 21, 80333 Muenchen, Germany
[b]BMW Group, Petuelring 130, 80809 Muenchen, Germany
[c]Technical University of Denmark, Anker Engelunds Vej 101, 2800 Kongens Lyngby, Denmark

ABSTRACT

The state-of-the-art position of cameras in forward-facing Advanced Driver Assistance Systems (ADAS) is behind the windshield, integrated within the rearview mirror holder. In this position, the quality of the windshield as an optical element directly impacts the quality of the camera image. With increasing camera resolution and narrow field of view optics required for large object detection distances, the optical impact of the windshield becomes increasingly important. We suggest a method based on computer graphics for evaluating the optical performance of windshields in front of ADAS cameras. Using a ray tracing framework, we produce quantitative simulations of the light transport through the windshield. To represent the geometry of the windshield, we fit ellipsoid models to measurements of its inner and outer surfaces produced using a chromatic white light sensor in a coordinate measuring machine. The ellipsoid fits enable accurate ray intersections with the windshield even for cameras positioned close to the windshield surface. Additionally, we investigate the windshield microgeometry using optical profilometry and find that the microstructure is smaller than 200 nm. Thus, the microgeometry can only cause a very slight diffractive blur, and we consider the ellipsoidal macrogeometry sufficient for evaluating the light transport. In simulation experiments, we evaluate the impact of the windshield on a forward-facing ADAS camera by computing the modulation transfer function degradation of the camera image. In our experiments, we vary camera aperture and resolution as well as distance and angle of the windshield to the camera. To validate our results, we reconstruct the angle variation experiment in the lab.

Keywords: ADAS cameras, windshield optical impact, windshield MTF, curved glass, ellipsoid fit

1. INTRODUCTION

Automotive advanced driver assistance systems (ADAS) continue to expand their capabilities, in terms of the different driving tasks they can handle, their level of automation, as well as their availability in different driving conditions. This evolution paves the way to full automation. To enable these advancements, ADAS functions impose increasing requirements on the sensor system of the vehicle. One of the main data sources are forward-facing cameras. A key requirement for these cameras is to resolve higher spatial frequency details, i.e. enabling detection of small objects at larger distances.

The state-of-the-art position of forward-facing ADAS cameras is behind the windshield, where the camera is integrated in proximity of the rearview mirror holder at the top edge of the windshield. This position generally offers few occlusions in the field of view (FoV) and inconspicuous integration within the vehicle design, and it allows use of the windshield heating and cleaning systems to sustain camera availability. However, it makes the windshield a part of the optical path of the camera. The quality of the windshield as an optical element directly impacts the quality of the camera image, which is challenging for two main reasons:

1. The windshield design and fabrication process is primarily tailored for mass production of a large sheet of curved, laminated glass that must fulfill strict automotive safety and durability requirements.[1] Additional design goals for optical quality with respect to a camera lens that is positioned close to the windshield surface are not easily met.

---

2. The windshield is typically not in scope of the design process of the optical path of the camera. The camera mount tolerances are significantly larger than those used in the camera lens design. Moreover, automotive manufacturers typically equip several vehicle models (with different windshields) with the same cameras.

With increasing camera resolution and narrow-FoV optics for the required large detection ranges, the optical impact of the windshield becomes increasingly important. The capability of the camera to resolve high spatial frequencies could become limited by refraction at the curved windshield, and additionally by aberrations due to local windshield imperfections. In this work, we present a first approach to evaluating the optical performance of windshields with respect to ADAS forward-facing cameras that is based on computer graphics methods. A different approach is presented by Krebs et al.,[2] who use an optical model of the windshield based on wavefront measurements to simulate the optical distortion of exemplary windshields. This requires a large set of wavefront measurements that depend on camera placement and FoV. In contrast, our approach uses ray tracing methods which can produce quantitative simulations of light transport using geometry and material models of the interacting objects. This means that once we have constructed and validated our windshield model, it can be used for arbitrary camera models and camera placement in front of the windshield. We introduce all components of our windshield model in Sections 2.1 and 2.2. We then present several simulation experiments in Section 2.3, in which we alter camera parameters and camera/windshield positioning and evaluate the impact of the windshield on the camera image. Our metric of optical impact is the degradation of the modulation transfer function (MTF).[3] The MTF measures the ability of the camera to resolve contrasts of objects depending on their spatial frequency. For validation of the simulation results we reconstruct one of the experiments in the lab as described in Section 2.4. The results of simulation and validation experiments follow in Sections 3.1 and 3.2. Examples of simulated camera images from our experiments are in Fig. 1, where Fig. 1b visibly exhibits loss of contrast at the edges of the rotated squares used for MTF calculation.

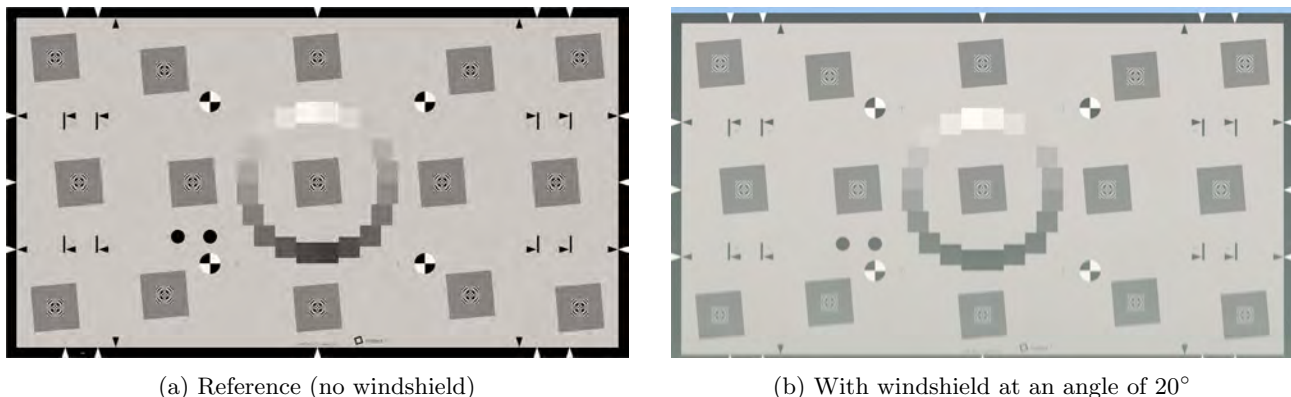| (a) Reference (no windshield) | (b) With windshield at an angle of 20° |

Figure 1: Simulation result exemplifying the optical impact of a windshield. At a small angle, the windshield clearly produces a reduced contrast at the slanted edges of the rotated squares of the ISO 12233:2017 edge spatial frequency response (eSFR) chart,[4,5] when compared to the reference image without windshield. The vertical shift of the image is caused by the windshield as well and should be accounted for in extrinsic camera calibration, but the focus in this work will be MTF degradation. High dynamic range (HDR) images were in this figure compressed for visualization. The windshield angle is defined in Section 2.3. The charts shown in this figure are products of Imatest LLC (https://www.imatest.com/).

2. METHODS

We represent the camera window section of the windshield as well as camera imaging sensor (imager) and lens using computer graphics models suitable for ray tracing methods. Ray tracing simulations are capable of producing physically correct optical images, i.e. representations of the irradiance that hits the imager.[6,7] Our core rendering framework is Mitsuba Version 0.5.0.[8]

2.1 Windshield Macrogeometry Model

At a macroscopic level, the windshield is a three-dimensional glass element with curved outer surfaces and approximately constant thickness. Automotive windshields are typically produced as laminated glass consisting of two outer glass elements and a thermoplastic polymer core.

We use a 3D model of the camera window of a state-of-the-art automotive windshield to represent the geometry of the windshield surfaces. The model was produced using a chromatic white light sensor (ZEISS DotScan) in a coordinate measuring machine,[9] i.e. measurements of both surface geometries are produced in a common reference coordinate system and hence automatically aligned. The surface geometry is scanned on a surface sampling grid with a resolution of 1 mm in each direction. We neglect the inner boundaries of the windshield between the laminate layers. The polymer layer typically has an index of refraction that is matched to that of the glass layers to minimize optical effects at the boundary. For the same reason, it is difficult to precisely measure the geometry of those boundaries using optical methods.

ADAS cameras are typically positioned close to the windshield in order to minimize the size of stray light covers and the size of the camera mount and housing on the vehicle interior. The closest distance between camera lens and interior windshield surface can be in the range of few millimeters. To achieve realistic rendering results, we need very accurate ray intersections with the windshield surface because slight deviations in transmissive paths close to the camera will lead to significantly divergent paths in the scene. For this reason, using the polygon mesh of the windshield camera window 3D model directly as macro model geometry does not give plausible results. For details see Appendix A.1.

Instead of using the discrete 3D model directly, we use the measurement points of each windshield surface as a 3D point cloud and fit an ellipsoid model with two independent radii to the points. The two independent radii represent the horizontal and vertical curvature of the windshield. Details on the ellipsoid fit are in Appendix A.2. We then export the ellipsoid fits of both surfaces to surface geometry models in Mitsuba scene descriptions using the sphere intersection primitive encapsulated in a shape group, and object-to-world transformations that translate and scale the unit sphere according to the ellipsoid model center and radii. Using sphere primitives to model geometries of optical elements is a commonly used approach in ray tracing and can for example be found in PBRT's *realistic camera* model.[6, 10] In Ref. 11, a spherical windshield model is used to derive an approximation of windshield refraction for automotive camera calibration.

This method can also be used based on windshield 3D models from other sources, e.g. computer-aided design (CAD) data, as long as it contains sufficiently precise data points of both windshield surfaces for accurate ellipsoid fits. If the 3D model contains the boundaries between the laminate layers, these can be added to the macrogeometry model.

2.2 Windshield Microgeometry Model

In addition to the macrogeometry model, we investigate the windshield microgeometry. A separation of geometric detail into separate models at different scale is a commonly used approach in computer graphics and allows adding effects of small-scale geometry that cannot be included in the macrogeometry model directly. Height field or normal map models as in Refs. 12, 13 allow to include microgeometry information that is sampled on small patches of the overall object surface only. When microgeometry structures are at the scale of the wavelengths of the light used for observation, diffraction models as in Refs. 14, 15 are required.

We use an optical profilometer (Zygo Nexview™ NX2) to record the height field of windshield surface patches that are approximately 0.84 mm by 0.84 mm large, at sub-micrometer surface resolution and sub-nanometer height information resolution. We postprocess the measurement data using filters for measurement noise, as well as second order polynomial components of the height map that represent macrogeometry information. We record height fields of exterior and interior surfaces of three sample windshields of the same windshield model at several locations each. One of these samples is also used for the macrogeometry measurement. The height fields of all measurements are consistent, and two examples from exterior and interior surface are shown in Fig. 2. They contain structures with a peak-to-valley height range of less than 20 nm on the exterior surface and less than 200 nm on the interior surface. These structures can only cause a very slight diffractive blur, and we consider the ellipsoidal macrogeometry sufficient for evaluating the light transport.
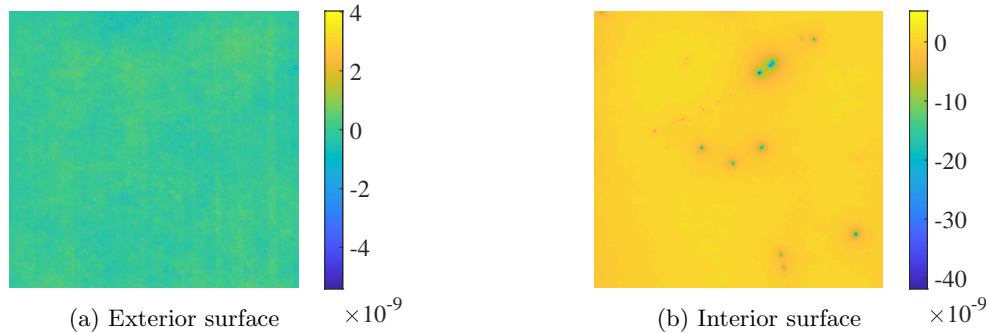
Figure 2: Microgeometry model: Exemplary measured height fields of both windshield surfaces. Height field dimensions are 0.84 mm by 0.84 mm. Height information scaled to meters.

2.3 Simulation Experiments

In our simulation experiments, we evaluate the impact of the windshield on a forward-facing ADAS camera in terms of the MTF degradation of the camera image. We quantify the MTF degradation as the drop of contrast in the MTF (MTF drop) at 0.25 lp/px (line pairs per pixel), i.e. the spatial frequency that corresponds to half the Nyquist limit of the imager; For each test scene we obtain a test MTF and a reference MTF, where the reference scene equals the test scene without the windshield model.

As camera model, we use Mitsuba's thin lens model with high dynamic range film. The thin lens model allows to simulate camera lenses with a specific aperture radius. We set the camera horizontal FoV to 30°, a typical value for narrow-FoV forward-facing ADAS cameras. Our windshield model is completed by a dielectric material model that represents the bidirectional scattering distribution function (BSDF) at the intersection of air and the windshield glass, defined by their indices of refraction. For the windshield glass, we use an index of refraction of 1.522. We neglect the absorption of the windshield.

We place the windshield model in front of the camera at a defined angle and distance between camera lens and interior windshield surface. For definition of the windshield angle, assume a Cartesian coordinate system in which the xz-plane is parallel to the ground plane and hence the y-axis defines the vertical direction. Assume the viewing direction of the camera is parallel to the z-axis. In this coordinate system, we define the windshield angle as the angle between the viewing direction of the camera (the z-axis) and the tangent of the interior windshield surface in the yz-plane. A vertical windshield corresponds to a windshield angle of 90° for this definition, and a nearly horizontal windshield corresponds to a small windshield angle. For definition of the distance between lens and windshield, we make the simplifying assumptions that the radius of the front lens equals the aperture radius, and that the lens is closest to the windshield at the top edge of the front lens. We find the closest point to the lens on the ellipsoid fit of the interior windshield surface in the yz-plane to calculate the distance.

Our MTF evaluations are based on capturing the ISO 12233:2017 eSFR chart[5] in the test scene. The chart (see Fig. 1) contains a 3-by-5 matrix of slightly rotated squares, the slanted edges of which are used as regions of interest (ROIs) for MTF measurement.[4] For our evaluations of the MTF drop we give the minimum, mean and maximum values over all horizontal and vertical MTF ROIs respectively. We place the test chart at the chosen focus distance of the camera model (300 cm) and scale it to fill the FoV of the camera. We rasterize the original vector graphics eSFR chart to a texture at a resolution that corresponds to a 2x oversampling of the maximum sensor resolution that we use in our experiments. The scene is illuminated by Mitsuba's automatically added natural lighting.

In the default scene configuration the camera has an aperture radius of 7.5 mm and a 4K film resolution. The windshield is set to an angle of 30° and a distance of 2 mm between camera lens and windshield interior surface. In this test scene, we define the following experiments:

- Angle experiment: We decrease the angle of the windshield from 80° to 20°, readjusting the windshield position at each tested angle to keep the lens - windshield distance fixed.

- Distance experiment: Starting from the initial windshield position, we shift the windshield along the line of sight of the camera to increase the distance between lens and windshield. In our experiments, the shift ranges from 0 mm to 50 mm.

- Aperture experiment: We increase the camera aperture radius from 2.5 mm to 10 mm and shift the windshield to keep the lens - windshield distance fixed with increasing lens radius (according to our assumption of equal aperture and lens radii).

- Resolution experiment: We increase the film resolution, using typical 16:9 imager resolution formats from HD to 8K.

2.4 Validation Experiment

To validate our simulation results we reconstruct the angle simulation experiment in a lab environment using a state-of-the-art ADAS camera as well as one of our windshield samples on a custom holder that allows to adjust the windshield angle. For the test scene we use a printed eSFR chart illuminated by LED lighting. The chart also shown in Fig. 3 has a different aspect ratio than the one used in the simulation experiment and hence different positions of the first and last column of rotated squares for MTF measurement. We exclude those two columns from our MTF measurements. We capture 8 bit raw images and apply a demosaicking and a color transformation adapted to the color filter array of the camera to obtain RGB images. We adapt the camera and target models in the simulation to match the available equipment. The setup of the validation experiment is shown in Fig. 3. Most importantly for our camera model, the camera has a smaller aperture radius, which we calculate as the effective focal length divided by two times the f-number,[3] and a larger field of view, which results in a smaller image resolution covered by the chart.

For angles of 30° or smaller, due to the size of camera housing and holder we cannot place the camera lens as close to the windshield as in our simulation. In these cases, we place the camera so that the lens is as close to the windshield as possible.

(a) Captured image (full FoV, raw visualized at reduced resolution)

(b) Captured image (cropped FoV, after demosaicking and color transformation)

(c) Simulated image (HDR compressed for visualization)

Figure 3: Setup for validation. Exemplary images for a windshield angle of 30°. The charts shown in this figure are products of Imatest LLC (https://www.imatest.com/).

3. RESULTS

3.1 Simulation Experiments

For the angle experiment, the results in Fig. 4 show the expected increasing vertical MTF degradation for decreasing windshield angles. For angles of 30° or smaller, the MTF drop saturates due to the limited reference MTF. The horizontal MTF is affected as well, especially at angles of 30° or smaller.

The results on the distance experiment in Fig. 5 indicate no sensitivity of the MTF drop on lens-windshield distance. Note that the vertical MTF drop is at a high level due to the default scene configuration. For a windshield with non-negligible microgeometry, a dependence of MTF degradation on the lens-to-windshield distance may exist.

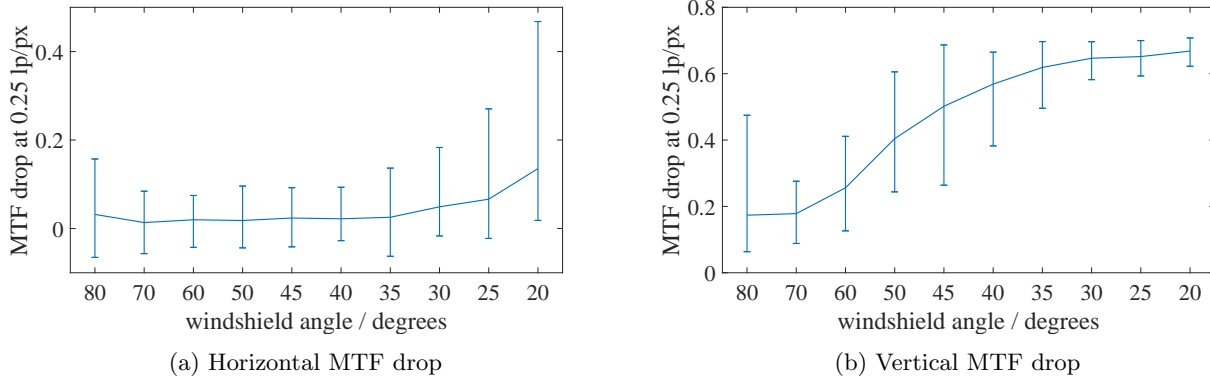(a) Horizontal MTF drop　　　　　　　　(b) Vertical MTF drop

Figure 4: MTF drop in angle experiment. A higher MTF drop means larger MTF degradation, hence a more severe optical impact of the windshield on the camera image. Note the nonuniform x-axis scaling due to the chosen exemplary windshield angles in the experiment.
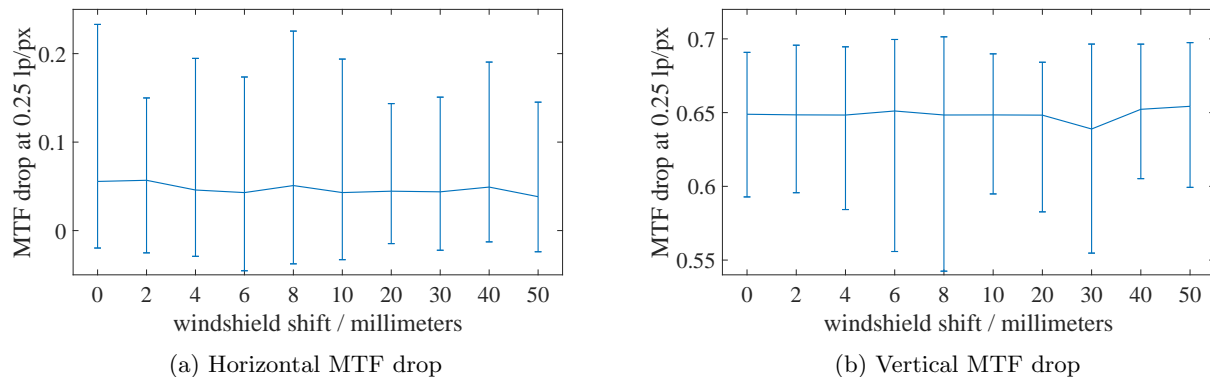

(a) Horizontal MTF drop　　　　　　　　(b) Vertical MTF drop

Figure 5: MTF drop in distance experiment. Note the nonuniform x-axis scaling due to the chosen exemplary windshield shifts along the line of sight of the camera.

The aperture experiment indicates increasing horizontal and vertical MTF degradation with increasing aperture, see Fig. 6. The increase of horizontal MTF drop is nearly linear, the increase of vertical MTF drop saturates due to the default windshield angle and imager resolution.

The results of the resolution experiment in Fig. 7 exhibit similar effects with increasing imager resolution as in the angle experiment with decreasing windshield angle. However, the maximum vertical MTF drop appears independent of the imager resolution and beyond saturation of the vertical MTF drop a slight decrease can be observed, which is possibly due to limited chart texture resolution in the simulation model.
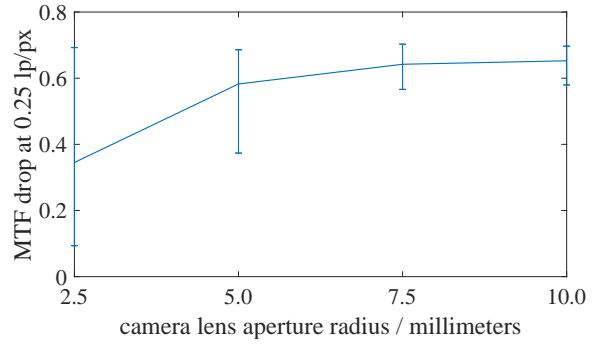
3.2 Validation Experiment

The simulation results of the validation experiment, see Fig. 8, indicate the same effects of the windshield angle on horizontal and vertical MTF drop as in the original angle experiment. The absolute values of the MTF drop are smaller for the camera and chart models that are matched to the hardware setup, than for the settings used in the original angle experiment.

The results of the validation measurements in Fig. 9 indicate increasing vertical MTF drop and slightly increasing horizontal MTF drop with decreasing windshield angle as in the simulation. In general, be observe a good fit between simulation and measurements, but the results do not match perfectly. In simulation, the mean vertical MTF drop increases significantly for windshield angles of 25° or less, and in the measurements only for 20°. At a windshield angle of 20°, we observe a larger maximum vertical MTF drop in the measurements, than in simulation. Possible roots of the remaining discrepancies of the results are the thin lens model of our camera
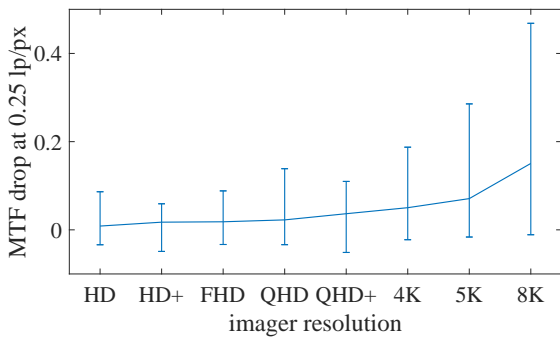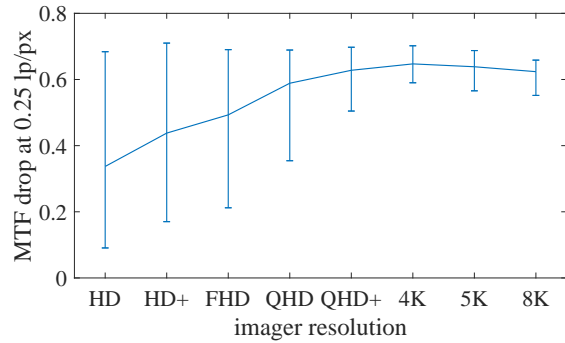
(a) Horizontal MTF drop   (b) Vertical MTF drop

Figure 6: MTF drop in aperture experiment.
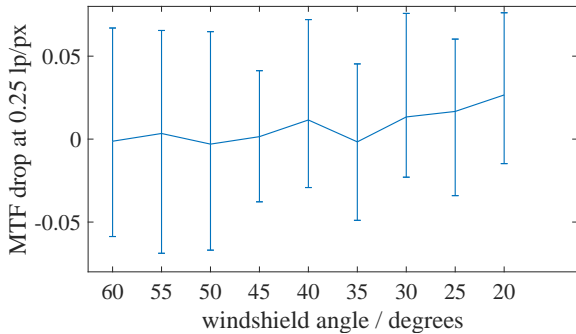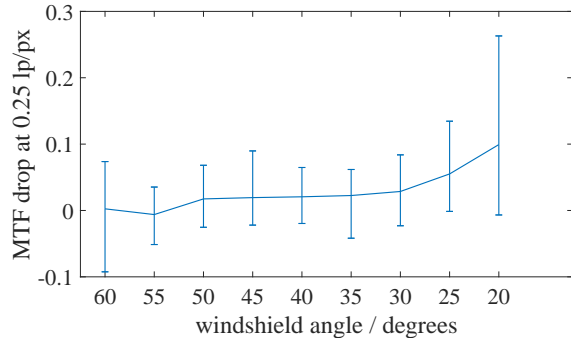

(a) Horizontal MTF drop   (b) Vertical MTF drop

Figure 7: MTF drop in resolution experiment. Note that the choice of typical imager resolutions results in a nonuniform x-axis scaling with respect to image width and height.

model, the practical restrictions to camera placement in the lab measurements for angles of $30°$ or less, as well as non-linear stages of the image capture and image processing in our lab measurements that are not reflected in our simulation model. In a first test, we investigated the impact of a gamma correction on the lab measurements to tune the image contrast, but found that it had little influence.

(a) Horizontal MTF drop   (b) Vertical MTF drop

Figure 8: MTF drop in simulation results of validation experiment. The validation experiment is a reconstruction of the angle experiment.
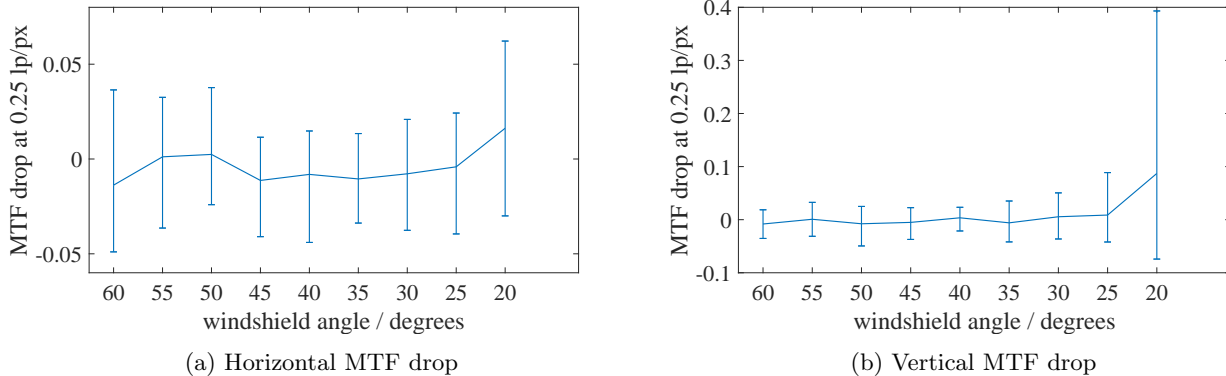
(a) Horizontal MTF drop   (b) Vertical MTF drop

Figure 9: MTF drop in lab measurements of validation experiment.

4. CONCLUSION

We presented an approach for modeling the optical impact of windshields on forward-facing ADAS cameras based on windshield macrogeometry measurements and ray tracing. We modeled the windshield surfaces using ellipsoid fits to a point cloud acquired using a coordinate measuring machine. Based on microgeometry measurements we found that for our windshield samples the impact of the microgeometry is negligible. We performed several simulation experiments showing the expected effects of varying windshield angle, lens-to-windshield distance, camera lens aperture, and imager resolution on the MTF performance of the camera. In a validation experiment, we found a good fit of our simulation results and lab measurements in terms of increasing vertical MTF degradation with decreasing windshield angle. However, the results did not match perfectly. Hence, further work is required to quantitatively reproduce the optical impact of the windshield using our simulation model. One may consider our current model a rough estimate of the MTF drop that a windshield can entail if placed at a given angle in front of an ADAS camera.

In future work, a camera model such as PBRT's *realistic camera* could be used to include more details of the camera lens stack. Also, the exposure configuration and image signal processing steps that can affect MTF measurements should be included in the model. For these reasons the windshield model should be embedded in a physically based camera simulation framework, e.g. the one proposed by us in Ref. 16.

An aspect that should be considered for the windshield model in future work is meso-level geometric information, i.e. surface geometry that is larger than the structures captured in the microgeometry measurements we use, but not represented in the ellipsoid fit macrogeometry model. The absorption of the windshield could be added using a medium model.

APPENDIX A. DETAILS ON MACROGEOMETRY MODELS

A.1 Models Directly Based on Measured 3D Model

Directly using the polygon meshes of the measured macrogeometry 3D models as windshield surfaces we could not achieve plausible rendering results, see Fig. 10. Even for the fine sampling grid of our chromatic white light sensor measurement data, the polygon facets that are close to the front lens of the camera create implausibly blurred images (Fig. 10b). Smoothing the polygon surface e.g. using Catmull-Clark subdivision does not resolve this effect but introduces further blur (Fig. 10c). We expect that this is the result of the smoothing effectively deforming the macroscopic surface.

A.2 Models Based on Ellipsoid Fits

For the ellipsoid fit we use the implementation in Ref. 17, constraining the ellipsoid to two equal radii and a third independent radius. The two equal radii are aligned with the axes that form the horizontal plane, the third radius is aligned with the vertical axis. In the process of the ellipsoid fit, we first rotate the measured 3D model to the chosen windshield angle and subsequently compute the surface fits for both windshield surfaces.
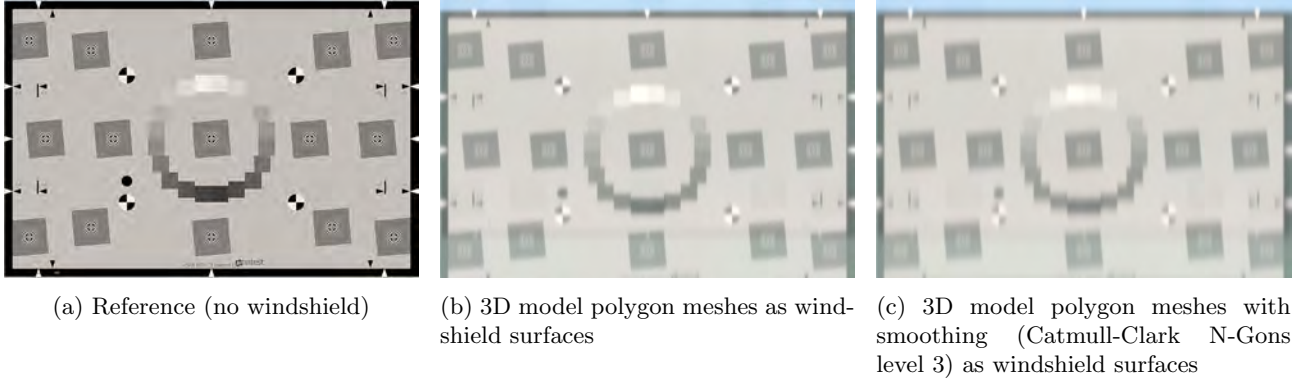
(a) Reference (no windshield)

(b) 3D model polygon meshes as windshield surfaces

(c) 3D model polygon meshes with smoothing (Catmull-Clark N-Gons level 3) as windshield surfaces

Figure 10: Macrogeometry model: Direct use of the measured 3D model for the windshield surfaces leads to implausible blur. Surface smoothing by Catmull-Clark subdivision adds additional blur. The charts shown in this figure are products of Imatest LLC (https://www.imatest.com/).
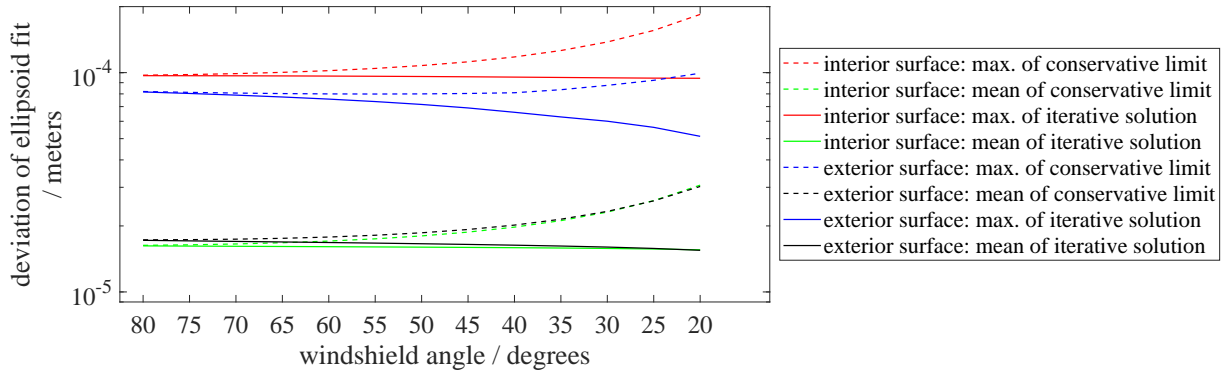

Figure 11: Ellipsoid fit quality measured as deviation of the ellipsoid surface from the surface measurement points. The mean and maximum values of both estimates are given for both windshield surfaces. Note the logarithmic scaling of the y-axis.

Especially since we generate new fits for each windshield angle, we evaluate the quality of the fits in terms of the deviation of the fitted surface from the measured 3D model, i.e. the distance of the measurement points to the ellipsoid surfaces. Calculating these distances requires finding the points on the ellipsoid surface that are closest to the measurement points. To give a conservative upper limit of the deviation we estimate the closest points by transforming the coordinate system to a space in which the ellipsoid surface becomes a unit sphere, finding the closest points on the unit sphere, and transforming back to the original coordinate system. This procedure is an adaptation of the residual sum of squared errors calculation in Ref. 17. For a closer limit of the deviation, we additionally use the algorithm in Refs. 18, 19, which uses an iteration to find the closest points to the measurement points on the ellipsoid surface. We run the algorithm for a maximum of 100 iterations for each point, with the break-off threshold for the maximum norm of the iteration step set to 1×10^{-8} m. The resulting deviation estimates for all angles used in our experiments are in Fig. 11. The maximum deviations of both surfaces are in the order of $100\,\mu m$, and the mean deviations are in the order of $10\,\mu m$.

REFERENCES

[1] "Uniform provisions concerning the approval of safety glazing materials and their installation on vehicles," Regulation 43, OJ L 42 12.02.2014, Economic Commission for Europe of the United Nations (UN/ECE), CELEX: https://eur-lex.europa.eu/legal-content/EN/TXT/?uri=CELEX:42014X0212(01). Accessed: 07 August 2022.

[2] Krebs, C., Müller, P., and Braun, A., "Impact of windshield optical aberrations on visual range camera

based classification tasks performed by CNNs," in [*Proceedings of IS&T London Imaging Meeting 2021: Imaging for Deep Learning*], 83–87 (2021).

[3] Allen, E. and Triantaphillidou, S., [*The manual of photography*], Focal Press, Abingdon, U.K. and Burlington, MA, USA, 10th ed. (2011).

[4] MathWorks, "esfrChart." https://de.mathworks.com/help/images/ref/esfrchart.html (2021). Accessed: 07 August 2022.

[5] Imatest, "Mathworks, esfr." https://www.imatest.com/mathworks/esfr/ (2021). Accessed: 07 August 2022.

[6] Pharr, M., Jakob, W., and Humphreys, G., [*Physically Based Rendering: From Theory to Implementation*], Morgan Kaufmann, Boston, MA, USA, 3rd ed. (2016).

[7] Farrell, J. E., Catrysse, P. B., and Wandell, B. A., "Digital camera simulation," *Applied Optics* **51**(4), A80–A90 (2012).

[8] Jakob, W., "Mitsuba version 0.5.0." https://github.com/mitsuba-renderer/mitsuba (2014).

[9] Hocken, R. J. and Pereira, P. H., [*Coordinate Measuring Machines and Systems*], CRC Press, Boca Raton, FL, USA, 2nd ed. (2011).

[10] Pharr, M., "pbrt version 3." https://github.com/mmp/pbrt-v3 (2020).

[11] Verbiest, F., Proesmans, M., and van Gool, L., "Modeling the effects of windshield refraction for camera calibration," in [*Proceedings of European Conference on Computer Vision (ECCV)*], 397–412, Springer International Publishing (2020).

[12] Dong, Z., Walter, B., Marschner, S., and Greenberg, D. P., "Predicting appearance from measured microgeometry of metal surfaces," *ACM Transactions on Graphics* **35**(1, article 9), 1–13 (2015).

[13] Wang, B., Hašan, M., Holzschuch, N., and Yan, L.-Q., "Example-based microstructure rendering with constant storage," *ACM Transactions on Graphics* **39**(5), 1–12 (2020).

[14] Yan, L.-Q., Hašan, M., Walter, B., Marschner, S., and Ramamoorthi, R., "Rendering specular microgeometry with wave optics," *ACM Transactions on Graphics* **37**(4), 1–10 (2018).

[15] Falster, V., Jarabo, A., and Frisvad, J. R., "Computing the bidirectional scattering of a microstructure using scalar diffraction theory and path tracing," *Computer Graphics Forum* **39**(7), 231–242 (2020).

[16] Weikl, K., Schroeder, D., Blau, D., Liu, Z., and Stechele, W., "End-to-end imaging system optimization for computer vision in driving automation," in [*Proceedings of IS&T Int'l. Symp. on Electronic Imaging: Autonomous Vehicles and Machines*], (2021).

[17] Petrov, Y., "Ellipsoid fit." https://www.mathworks.com/matlabcentral/fileexchange/24693-ellipsoid-fit, MATLAB Central File Exchange (2015). Accessed: 07 August 2022.

[18] Bektas, S., "Orthogonal distance from an ellipsoid," *Boletim de Ciências Geodésicas* **20**(4), 970–983 (2014).

[19] Bektas, S., "shortest_distance(X, axis)." https://de.mathworks.com/matlabcentral/fileexchange/46261-shortest_distance-x-axis, MATLAB Central File Exchange (2017). Accessed: 07 August 2022.